Published in final edited form as:
Biochemistry. 2008 September 23; 47(38): 9934–9936. doi:10.1021/bi801315m.

pH Induced Conformational Change of Influenza M2 Protein C-terminal Domain†

Phuong A. Nguyen[‡], **Cinque S. Soto**[§], **Alexei Polishchuk**[§], **Gregory A. Caputo**[§], **Chad D. Tatko**[§], **Chunlong Ma**[‖], **Yuki Ohigashi**[‖], **Lawrence H. Pinto**[‖], **William F. DeGrado**[*,§], and **Kathleen P. Howard**[*,‡]

[‡]Department of Chemistry and Biochemistry, Swarthmore College, Swarthmore PA 19081

[§]Department of Biochemistry and Biophysics, School of Medicine of the University of Pennsylvania, Philadelphia, PA 19104

[‖]Department of Neurobiology and Physiology, Northwestern University, Evanston, IL 60208

Abstract

The M2 protein from influenza A is a pH-activated proton channel that plays an essential role in the viral life cycle and serves as a drug target. Using spin labeling EPR spectroscopy we studied a 38-residue M2 peptide spanning the transmembrane region and its C-terminal extension. We obtained residue-specific environmental parameters under both high and low pH conditions for nine consecutive C-terminal sites. The region forms a membrane surface helix at both high and low pH although the arrangement of the monomers within the tetramer changes with pH. Both electrophysiology and EPR data point to a critical role for residue Lys 49.

M2 is a 96-residue homotetrameric integral membrane protein with a small N-terminal ectodomain, a single transmembrane helix and a C-terminal cytoplasmic tail. Despite data from solid state NMR (1), x-ray crystallography (2) and solution NMR (3), a detailed understanding of how the M2 protein works continues to puzzle investigators and generate sharp controversy.

The majority of published studies on the proton channel function of M2 have focused on the transmembrane (TM)[1] domain. However, truncation studies indicate that the cytoplasmic domain also plays a role in channel stability (4). Proteolysis of micelle-bound full length M2 revealed that a 15–20 residue segment C-terminal to the TM helix was highly protected from cleavage by proteases (5). Helical wheel analysis of the protected region (5) suggested that the segment could form an amphiphilic helix, consistent with later findings from solid state NMR on M2 protein in lipid bilayers (6). In order to further test the proposed models, we probed the conformation of the segment C-terminal to the TM domain at both high and low pH using site-directed spin-labeling (SDSL) and electron paramagnetic resonance (EPR) spectroscopy.

EPR studies were performed on a series of 38-residue synthetic M2 peptides (residues 23–60; M2TMC) spanning the TM region and the beginning of the C-terminal domain. We spin-

†This research was supported by R01AI57363 (LHP), GM56423 (WFD), a Henry Dreyfus Teacher Scholar Award (KPH) and R15AI074033 (KPH).

*To whom correspondence should be addressed: Kathleen Howard; E-mail: khoward1@swarthmore.edu. Phone: (610) 328-8519, Fax: (610) 328-7355. William DeGrado; Email: wdegrado@mail.med.upenn.edu. Phone: (215) 898-4590, Fax: (215) 573-7229.

[1]Abbreviations: CW, continuous wave; EPR, electron paramagnetic resonance; M2TMC, M2 peptide residues 23–60; MTSSL, 1-oxyl-2,2,5,5-tetramethyl-3-pyrroline-3-methyl methanethiosulfonate; NiEDDA, nickel(II) ethylenediamine-*N*,*N*'-diacetate; POPC, 1-palmitoyl-2-oleyl-*sn*-glycero-phosphocholine; POPG, 1-palmitoyl-2-oleyl-*sn*-glycero-3-[phospho-*rac*-(1-glycerol)]; RMSD, root mean square distance; SDSL, site-directed spin-labeling; TM, transmembrane domain

labeled nine consecutive sites (residues 48–56) immediately C-terminal to the TM region using cysteine-specific MTSSL spin labels (Figure S1). These labeling sites were chosen to probe two full turns of the proposed amphiphilic helix (5). To test the functional implications of the cysteine mutagenesis necessary for spin-labeling experiments, channel function of the relevant cysteine mutants was evaluated. Electrophysiology experiments on full-length M2 protein reveal that, out of the 9 spin-labeling sites (48–56), Cys substitution is detrimental to channel function only at one site (Lys 49), showing that this residue plays a critical role in the function of the channel (Figure 1). Cys substitution at the other 8 sites gives rise to channels with conductance and reversal potential properties very close to those observed for the wild-type channel.

Spin-labeled peptides were reconstituted into POPC/POPG (4:1) lipid bilayers and studied at both pH 7.8 and pH 5.6. At pH 7.8, the channel does not conduct protons. Lowering the pH to 5.6 activates the channel (7). Under both pH conditions, the following parameters were obtained using EPR: accessibility to a lipid-soluble paramagnetic reagent (O_2), accessibility to a water-soluble paramagnetic reagent (nickel(II) ethylenediaminediacetate, NiEDDA), and distance-dependent dipolar interaction between labels on neighboring monomers within a tetrameric bundle. These EPR parameters are sensitive reporters of secondary structure and protein topology and can be collected in a lipid bilayer environment at ambient temperature (8). Our data reveal that there are significant differences in the conformation of the C-terminal segment at pH 7.8 and pH 5.6.

Collision frequencies between the spin label and O_2 or NiEDDA were measured using power saturation techniques (9). Molecular oxygen is a small hydrophobic species that generally partitions into lipid bilayers, while water-soluble NiEDDA is located mainly in solution. Residue-by-residue patterns of measured accessibilities to O_2 and NiEDDA represent a blueprint of a protein's secondary structure and topology with respect to the membrane (10).

Figures 2C,D show the lipid (O_2) and water (NiEDDA) accessibility plots for the resting, non-conducting state at pH 7.8. Lipid accessibility data for the nine labeled sites show a sinusoidal variation typical for a surface absorbed α-helix. The water accessibility profile has the same periodicity, but is 180° out of phase to the lipid accessibility data. This 180° phase shift for water versus lipid accessibility is a signature of an amphiphilic helix associated with the membrane's hydrophobic/hydrophilic interfacial region (10). The lipid and water accessibilities match the physiochemical properties of individual amino acid side chains in the WT sequence. The most membrane-embedded residues (Phe 48, Ile 51, and Phe 55) are hydrophobic, while the most water-exposed residues (Lys 49 and Arg 53) are hydrophilic. Polar and apolar residues segregate to opposite faces of the helix (Figure S2).

M2 protein is a homotetramer in its native state (7). Whereas accessibility profiles allowed us to deduce the secondary structure and topology of individual helices with respect to the membrane, we must examine intersubunit proximities to determine the relative arrangement of the helical monomers within the tetrameric bundle. Intersubunit proximities are estimated from the distance-dependent interaction between spin labels on neighboring monomers. Through-space magnetic dipolar interaction between spin labels within ~8–20 Å leads to distance-dependent broadening of the CW EPR spectral line (11). A qualitative measure of interspin proximity is the interaction parameter (Ω) obtained as the ratio of central line amplitudes (M_I=0) of the spectrum of dilute-labeled channels and the broadened spectrum of fully labeled channels (12).

A profile of Ω at pH 7.8 (Figure 2E) versus the position of the spin label in the sequence shows two trends: 1) the profile peaks at residues 49, 52, and 55, roughly matching the period of an alpha helix; 2) the height of the peaks progressively decreases towards the C-terminal end of

the structure. The greatest interspin interaction occurs at residue 49, which is consistent with this residue playing a defining role at the end of the channel. We hesitate to over-interpret the data for this residue, however, because the K49C has impaired function. Of the remaining sites, Tyr 52 is closest to its cognate partners within the tetramer.

Very deep-seated differences in the EPR spectra occur when the pH is shifted to 5.6, which activates the channel for proton conduction. As observed at pH 7.8, the accessibility plots for lipid and water accessibilities are typical of an amphiphilic helix at the surface of a phospholipid bilayer (Figures 2C,D). However, there is a pronounced difference in the accessibilities of position 50, 52, 54, and 56, indicating that these sites become more deeply buried in the membrane at low pH (Table S1). Examination of physical models suggests that the observed changes in accessibility parameters upon lowering the pH might be accomplished by a clockwise rotation of the helix about its helical axis together with a small displacement of the helix center of mass to a deeper location in the bilayer. Indeed, the best-fit sine waves for both the O_2 and the NiEDDA data sets include both a change in y-offset, consistent with a helix sinking into the membrane, and a ~30° phase shift, consistent with a clockwise rotation about the helical axis (see Supporting Information for details). The helical wheel cartoons shown in Figure S2 depict a model for this pH induced conformational change.

Solution NMR spectra in micelles (3) and solid-state NMR spectra in bilayers (6) show only a single set of resonances from individual sites in M2 protein, consistent with a fourfold symmetric tetramer. In a tetrameric bundle with fourfold symmetry and right-handed arrangement of the C-terminal helices, a clockwise rotation would move the helices away from each other, predicting increased intersubunit distances between the helices consistent with predictions from crystallographic (2) and disulfide crosslinking studies (13). Except for the non-functional K49C mutant, we see no dipolar broadening in the C-terminal region at pH 5.6 indicating the helices are further apart than at pH 7.8 where significant interaction was seen at positions 51, 52, 53 and 55. Thus our model proposes that upon channel activation by low pH, the C-terminal helices move away from the center of the tetrameric bundle and become more embedded in the membrane. A strengthened association between the helix and the bilayer may be required to keep the channel open, explaining the premature closure of the channel truncated at Tyr 52 (4).

To provide an atomic model of the C-terminal region in the context of the transmembrane bundle, a model based on the crystal structure of the transmembrane region of M2 (2) was extended to include the cytoplasmic helix. A library of helix-loop-helix motifs was used as templates to direct the trial conformations for the loop and cytoplasmic helix. The resulting structures were quantitatively scored for their agreement with the EPR data using correlation methods. The ensemble RMSD of the top-scoring models using EPR data collected at pH 7.8 is 2.0 Å (see Supporting Information for details). The cytoplasmic helices fold into a square-like arrangement with their long axes parallel to the membrane surface (Figure S3). The helices interact with the membrane as well as the cytoplasmic ends of the neighboring TM helices. The C-terminal surface helices frame the cytoplasmic lumen of the channel proximal to the critical gating residues His 37 and Trp 41. Due to the lack of distance restraints, the family of structures at pH 5.6 is less well defined (ensemble RMSD = 3.5 Å) than at pH 7.8. Nonetheless, comparison of the pH 7.8 and pH 5.6 ensembles (Figure 3 and Figure 3S) shows that, on average, the C-terminal helices are further apart and deeper in the membrane at pH 5.6.

The structural features of the C-terminal helix in our EPR model show similarities as well as differences when compared to the solution NMR structure (3) of a peptide of similar length to the one studied here. Both studies suggest that the C-terminal region forms an amphiphilic helix, which lies nearly parallel to the membrane surface. However, the distances between symmetry-related residues in the NMR structure are poorly correlated with the relative

distances inferred from the EPR data (Figure S4). Differences between the NMR and the EPR structure likely reflect differences in the samples – our work focuses on peptide reconstituted in bilayer membranes in the absence of drug, while the NMR structure was solved in detergent micelles in the presence of the antiviral drug rimantadine.

While it has been known that the cytoplasmic membrane-proximal region of M2 is helical and that it is important for the stability and expression of the protein, its structure and functional role has been less well understood. Previously it was proposed that this region might either form a helical bundle, engaging in stabilizing helix-helix interaction, or that it might form a more rosette-like structure with the cytoplasmic helix hydrophobically interacting with the membrane bilayer (5). Solid-state NMR has provided support for the rosette model (6) while the solution NMR structure (3) showed features common to both models. Here we show that the C-terminal surface helix plays a more active role in the pH-activation process: residue Lys 49 is shown to be critical to the function of the channel, and we show that the entire region undergoes a conformational change, moving deeper into the bilayer in response to pH activation.

Supplementary Material

Refer to Web version on PubMed Central for supplementary material.

REFERENCES

1. Nishimura K, Kim S, Zhang L, Cross TA. The closed state of a H^+ channel helical bundle combining precise orientational and distance restraints from solid state NMR. Biochemistry 2002;41:13170–13177. [PubMed: 12403618]
2. Stouffer AL, Acharya R, Salom D, Levine AS, Di Costanzo L, Soto CS, Tereshko V, Nanda V, Stayrook S, DeGrado WF. Structural basis for the function and inhibition of an influenza virus proton channel. Nature 2008;451:596–600. [PubMed: 18235504]
3. Schnell JR, Chou JJ. Structure and mechanism of the M2 proton channel of influenza A virus. Nature 2008;451:591–595. [PubMed: 18235503]
4. Tobler K, Kelly ML, Pinto LH, Lamb RA. Effect of cytoplasmic tail truncations on the activity of the M2 ion channel of influenza A virus. J. Virol 1999;73:9695–9701. [PubMed: 10559278]
5. Kochendoerfer GG, Salom D, Lear JD, Wilk-Orescan R, Kent SB, DeGrado WF. Total chemical synthesis of the integral membrane protein influenza A virus M2: role of its C-terminal domain in tetramer assembly. Biochemistry 1999;38:11905–11913. [PubMed: 10508393]
6. Tian C, Gao PF, Pinto LH, Lamb RA, Cross TA. Initial structural and dynamic characterization of the M2 protein transmembrane and amphipathic helices in lipid bilayers. Protein Sci 2003;12:2597–2605. [PubMed: 14573870]
7. Pinto LH, Lamb RA. The M2 Proton Channels of Influenza A and B Viruses. J. Biol. Chem 2006;281:8997–9000. [PubMed: 16407184]
8. Fanucci GE, Cafiso DS. Recent advances and applications of site-directed spin labeling. Curr. Opin. Struct. Biol 2006;16:644–653. [PubMed: 16949813]
9. Altenbach C, Greenhalgh D, Khorana HG, Hubbell WL. A Collision Gradient-Method to Determine the Immersion Depth of Nitroxides in Lipid Bilayers. Proc. Natl. Acad. Sci. U. S. A 1994;91:1667–1671. [PubMed: 8127863]
10. Hubbell WL, Gross A, Langen R, Lietzow MA. Recent advances in site-directed spin labeling of proteins. Curr. Opin. Struct. Biol 1998;8:649–656. [PubMed: 9818271]
11. Klug CS, Feix JB. Methods and applications of site-directed spin Labeling EPR Spectroscopy. Biophysical Tools for Biologists: Vol 1 in Vitro Techniques 2008:617–658.
12. Mchaourab, HS.; Perozo, E. Determination of Protein Folds and Conformational Dynamics Using Spin-Labeling EPR Spectroscopy. In: Berliner, L.; Eaton, S.; Eaton, G., editors. Distance Measurements in Biological Systems by EPR. 2000. p. 185-247.

13. Bauer CM, Pinto LH, Cross TA, Lamb RA. The influenza virus M2 ion channel protein: probing the structure of the transmembrane domain in intact cells by using engineered disulfide cross-linking. Virology 1999;254:196–209. [PubMed: 9927586]

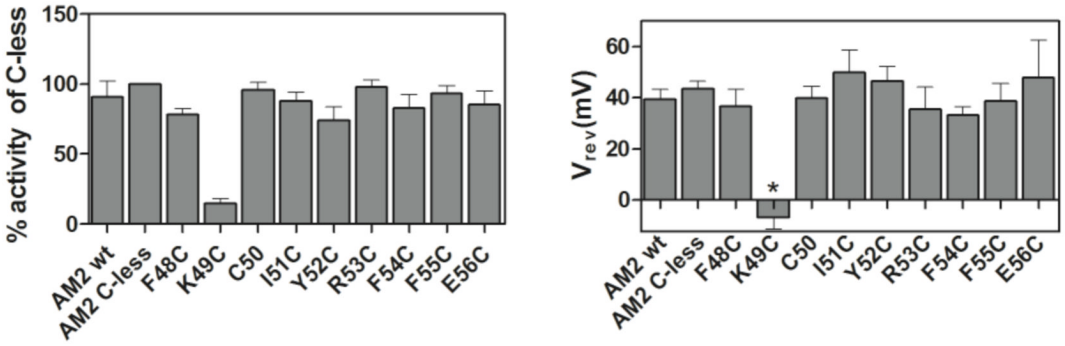

FIGURE 1.

Effect of cysteine substitutions on ion channel function of M2. Channel activity and reversal potential (V_{rev}) were measured at pH 5.5 in *Xenopus laevis* oocytes expressing full-length wild-type M2, cysteine-less M2, and M2 constructs derived from cysteine-scanning mutagenesis. * indicates that the V_{rev} of K49C construct could not be determined accurately due to its very low specific activity.

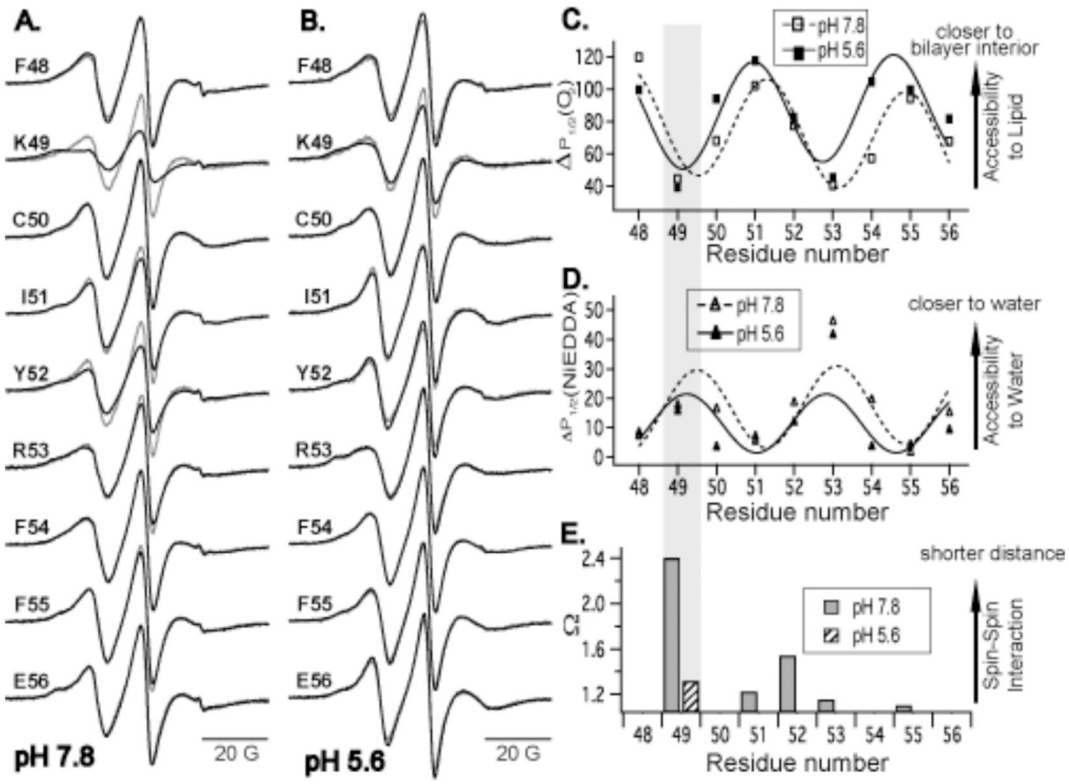

FIGURE 2.

pH-dependent conformational change. (A and B) CW-EPR spectra of spin labels at positions 48–56 on the M2TMC peptide reconstituted into POPC/POPG (4:1) lipid bilayers at pH 7.8 (A) and pH 5.6 (B). Overlay of spectra of fully labeled tetrameric channels (*black*) and spectra of dilute-labeled channels (*grey*). (C and D) Superposition of lipid (C) and water (D) accessibility profiles at pH 7.8 and pH 5.6. Details of best-fit sin waves to accessibility data are in the Supporting Information. (E) Superposition of per-residue intersubunit proximity patterns based on the interaction parameter measured at pH 7.8 and pH 5.6. Data for position 49 are boxed in grey to highlight that the K49C mutation causes loss of channel function.

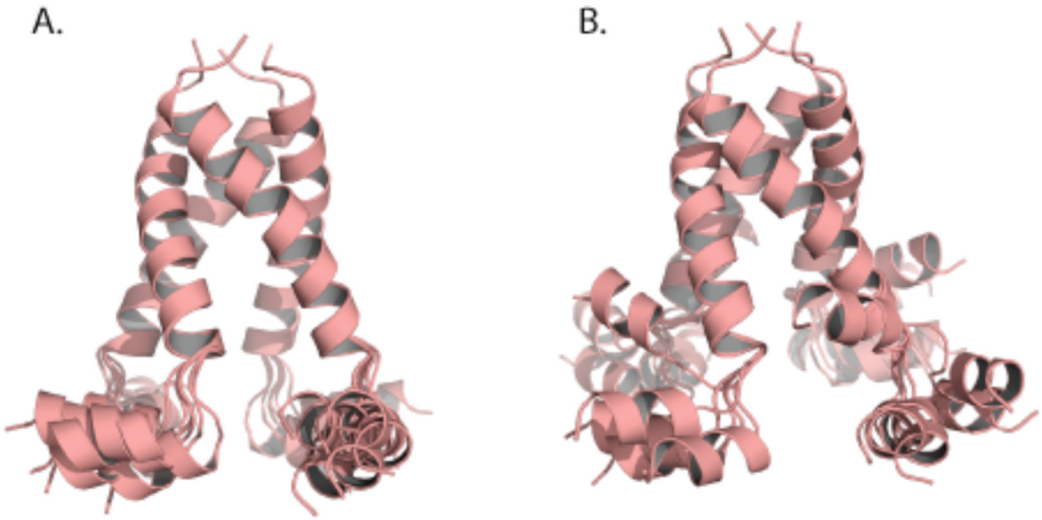

FIGURE 3.

Ensemble of models selected using EPR data. (A) Superposition of six most favorable scoring models using EPR data collected at pH 7.8 where the channel is in the resting, non-conductive state. (B) Superposition of six most favorable scoring models using EPR data collected at pH 5.6 where the channel is activated for proton conduction.